Supporting information

Anilido-Oxazoline-Ligated Rare-Earth Metal Complexes: Synthesis, Characterization and Highly *cis*-1,4-Selective Polymerization of Isoprene

Yu Pan,[a] Wenqiang Li,[a] Ning-Ning Wei,[b] Yat-Ming So,[c] Yang Li,*[a] Kang Jiang[a] and Gaohong He*[a]

[a] State Key Laboratory of Fine Chemicals, School of Petroleum and Chemical Engineering, Dalian University of Technology, Panjin, Liaoning 124221, China.

[b] School of Life Science and Medicine, Dalian University of Technology, Panjin, Liaoning 124221, China.

[c] Department of Chemistry, The Hong Kong University of Science and Technology, Clear Water Bay, Kowloon, Hong Kong, China.

*To whom correspondence should be addressed: E-mail: chyangli@dlut.edu.cn, hgaohong@dlut.edu.cn

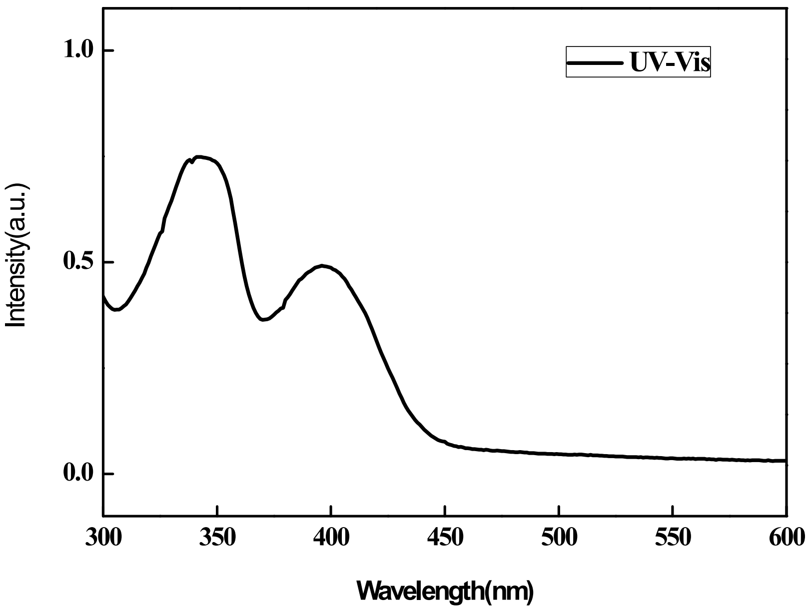

Fig. S1. UV-Vis spectrum of $L^1Sc(CH_2SiMe_3)_2THF$ (**1**) at 25 °C in hexane.

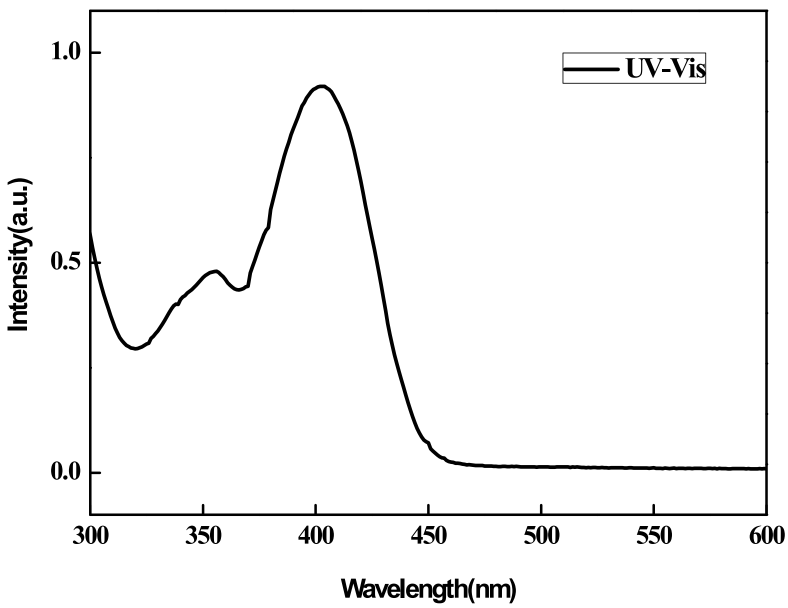

Fig. S2. UV-Vis spectrum of $L^2Sc(CH_2SiMe_3)_2$ (**2**) at 25 °C in hexane.

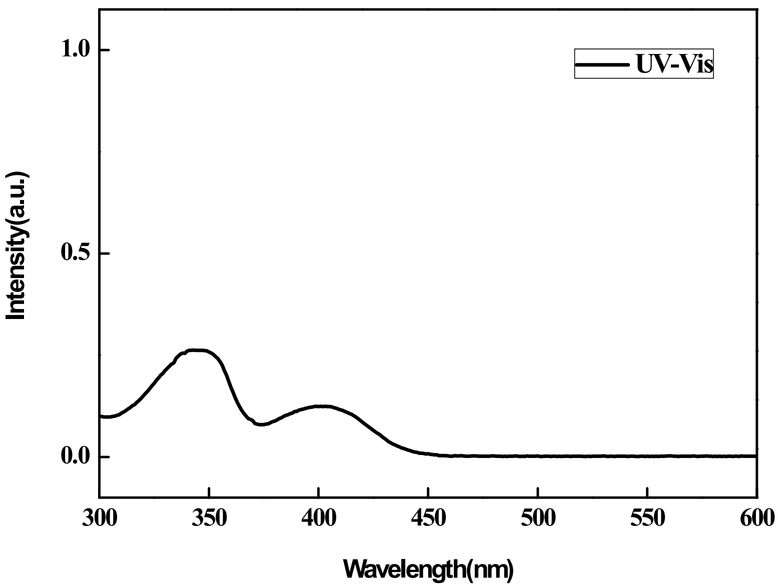

Fig. S3. UV-Vis spectrum of $L^1Y(CH_2SiMe_3)_2THF$ (**3**) at 25 °C in hexane.

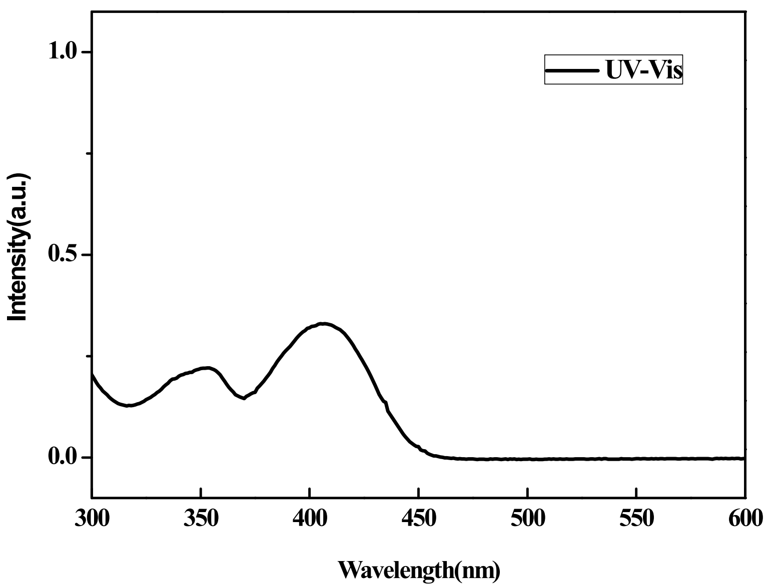

Fig. S4. UV-Vis spectrum of $L^2Y(CH_2SiMe_3)_2THF$ (**4**) at 25 °C in hexane.

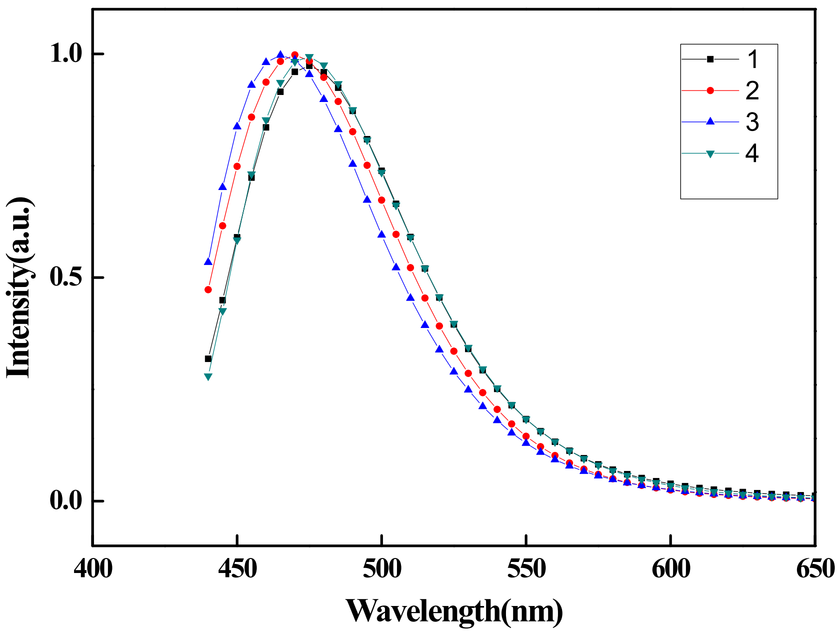

Fig. S5. Fluorescence emission spectra of complexes **1−4** at 25 °C in hexane.

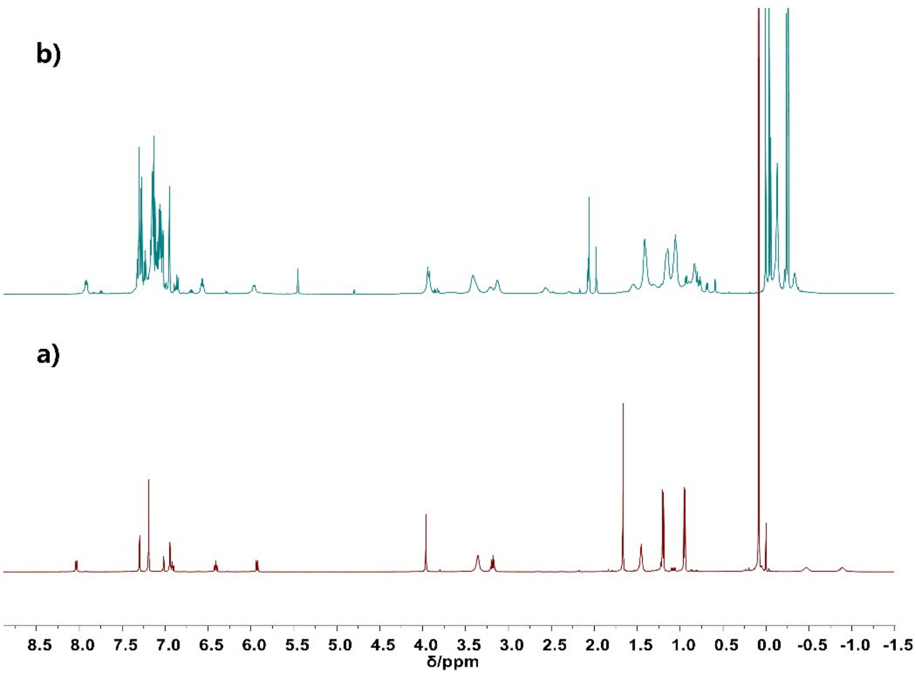

Fig. S6. [1]H NMR spectra (500 MHz, C_6D_5Br, 25 °C) of a) **4**; b) **4**/$[Ph_3C][B(C_6F_5)_4]$.

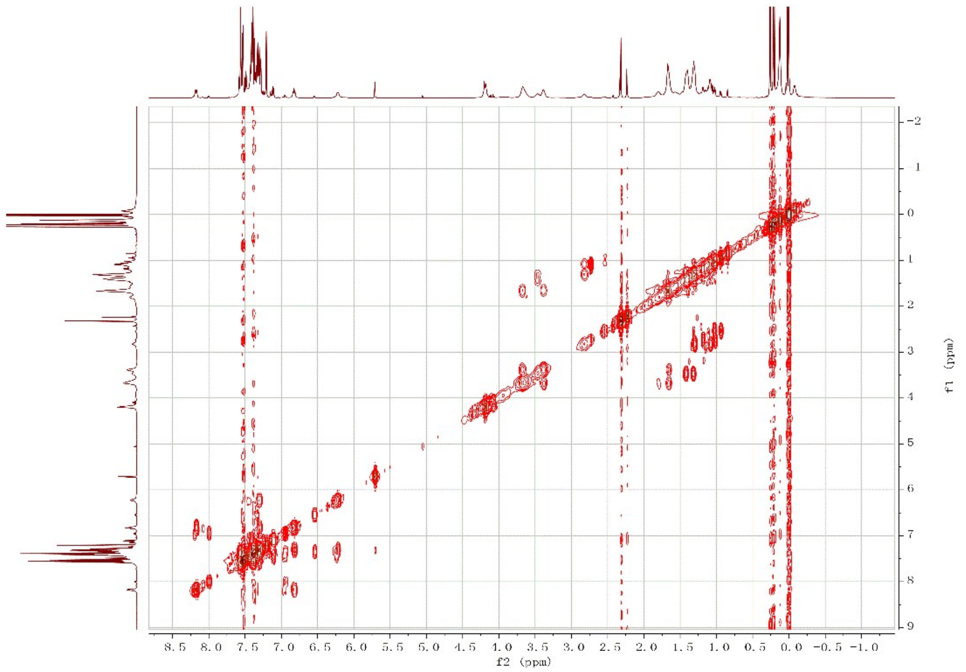

Fig. S7. ^{1}H-^{1}H COSY NMR spectrum of **4**/$[Ph_3C][B(C_6F_5)_4]$ in C_6D_5Br.

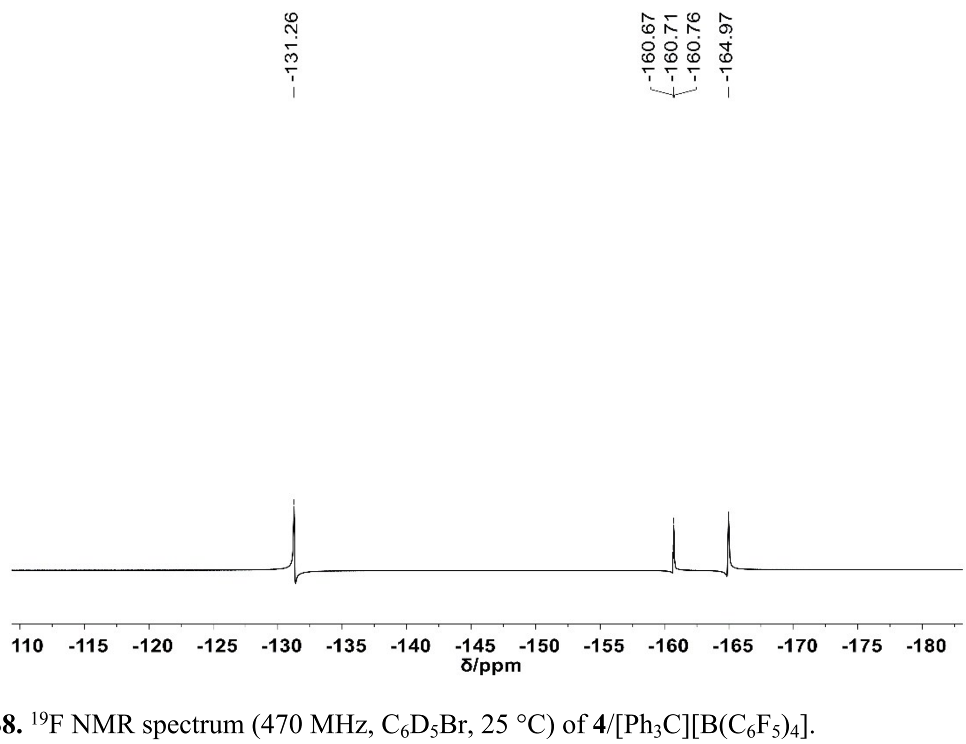

Fig. S8. ^{19}F NMR spectrum (470 MHz, C_6D_5Br, 25 °C) of **4**/$[Ph_3C][B(C_6F_5)_4]$.

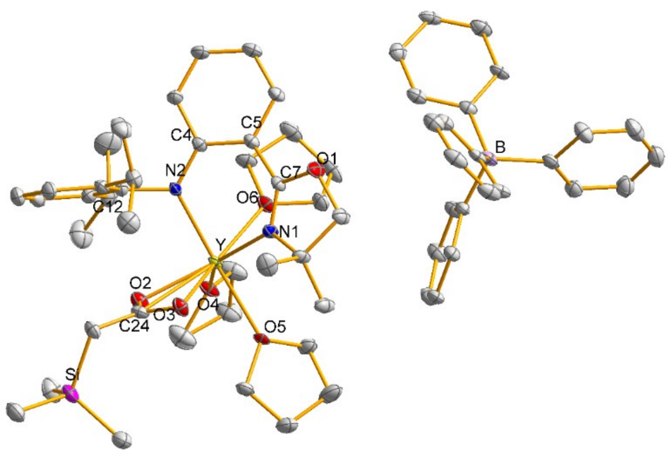

7

Fig. S9 Geometric structure of **7** (CCDC: 1880488). Hydrogen atoms are omitted for clarity. The ellipsoids are drawn at 30% probability level. Selected bond lengths (Å) and angles (°): Y-N(1) 2.3979, Y-N(2) 2.3152, Y-O(2) 2.2673, Y-O(3) 2.3519, Y-O(4) 2.4888, Y-O(5) 2.3871, Y-O(6) 2.4043, N(1)-C(7) 1.2896, N(2)-C(4) 1.3623, O(2)-Y-O(3) 56.396, O(2)-Y-C(24) 93.401, O(3)-Y-C(24) 90.389,N(2)-Y-O(4) 118.994,N(1)-Y-N(2) 77.517, O(2)-C(24)-O(3) 118.30, N(1)-Y-O(5) 92.960.

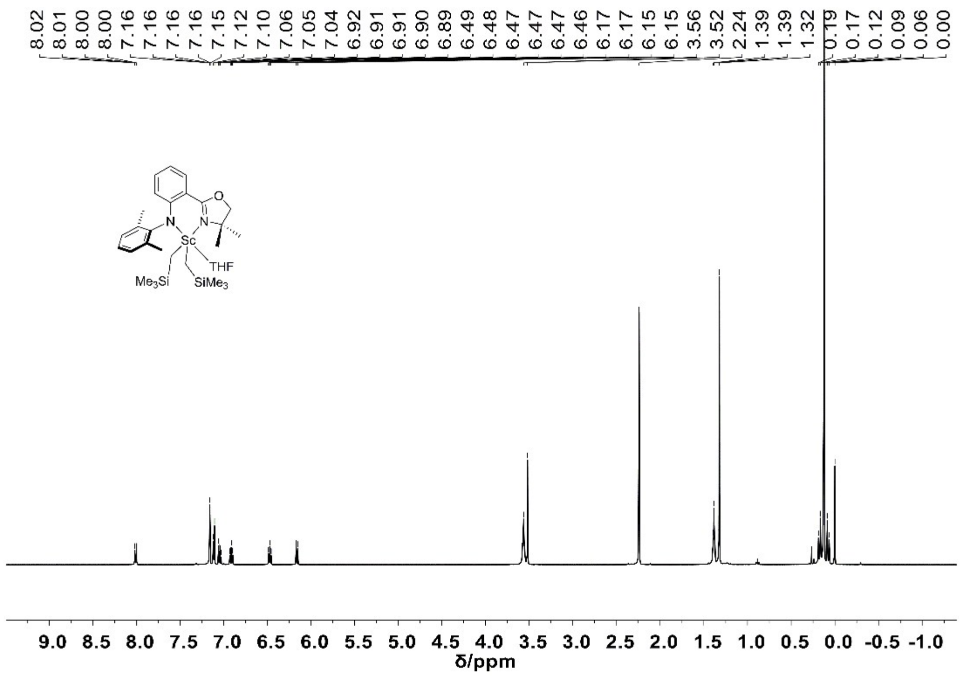

Fig. S10. ^{1}H NMR spectrum (500 MHz, C_6D_6, 25°C) of $L^1Sc(CH_2SiMe_3)_2THF$ (**1**).

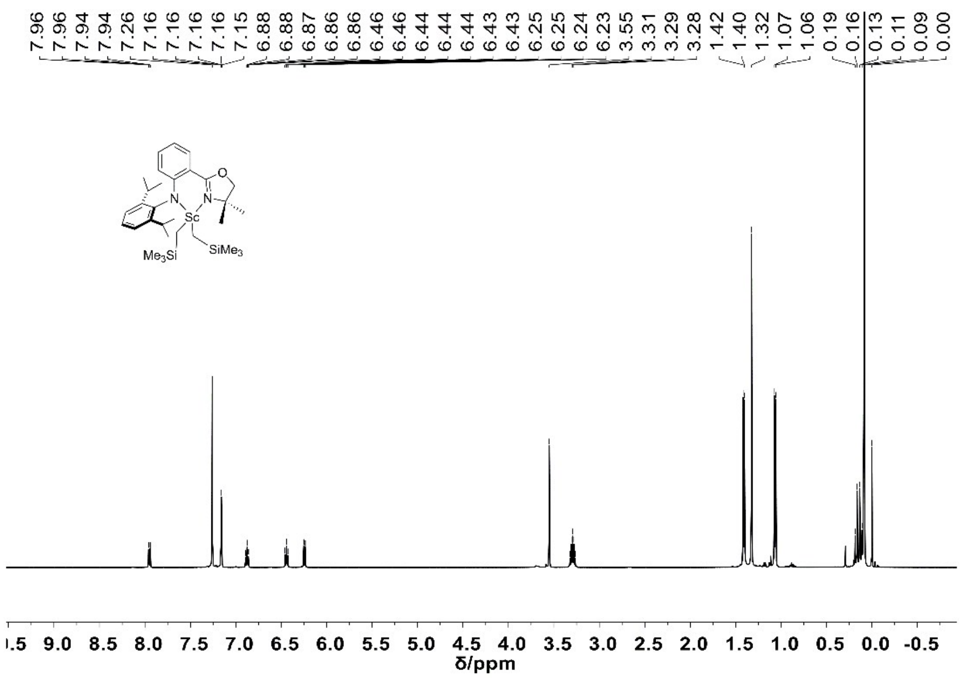

Fig. S11. ^{1}H NMR spectrum (500 MHz, C_6D_6, 25°C) of $L^2Sc(CH_2SiMe_3)_2$ (**2**).

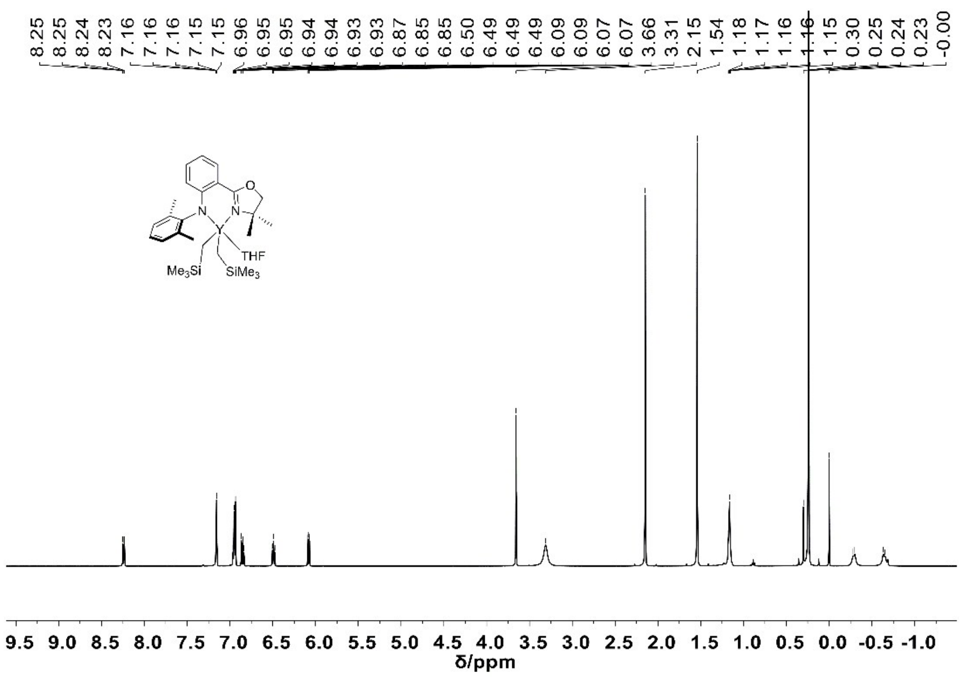

Fig. S12. ^{1}H NMR spectrum (500 MHz, C_6D_6, 25°C) of $L^1Y(CH_2SiMe_3)_2THF$ (**3**).

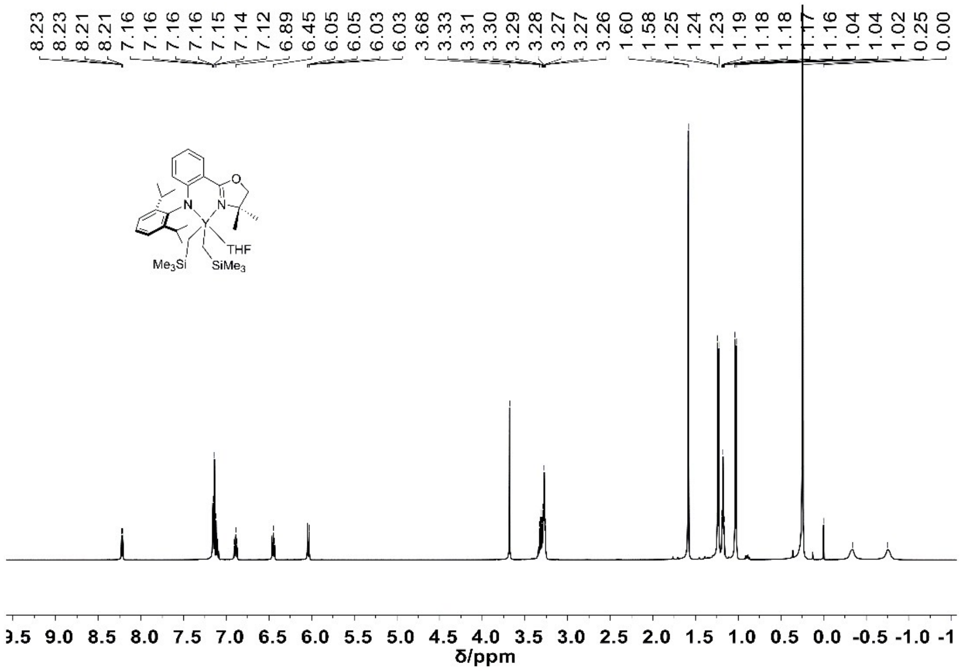

Fig. S13. ^{1}H NMR spectrum (500 MHz, C_6D_6, 25°C) of $L^2Y(CH_2SiMe_3)_2THF$ (**4**).

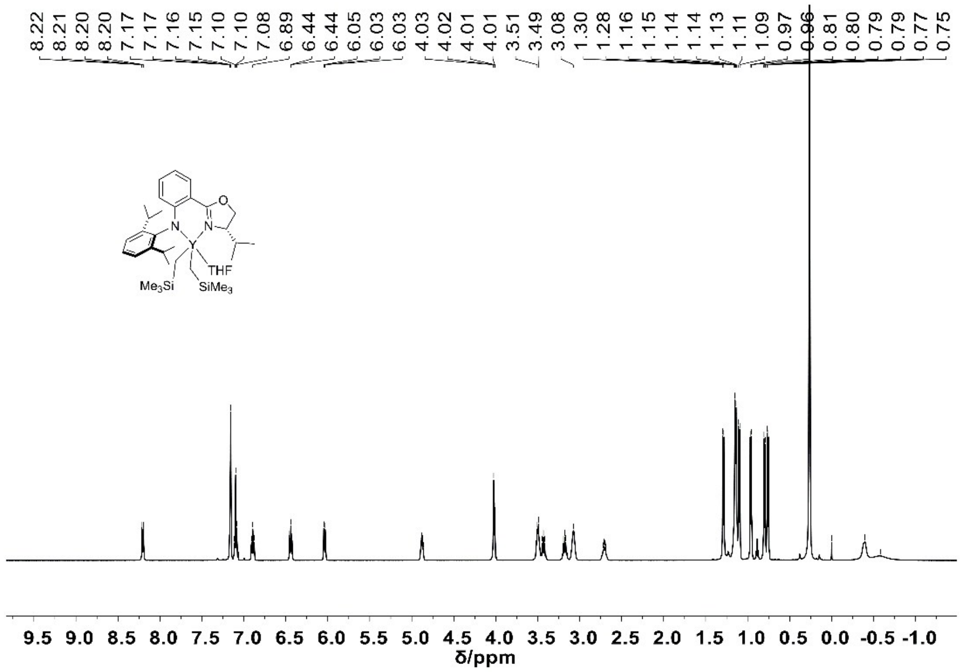

Fig. S14. ^{1}H NMR spectrum (500 MHz, C_6D_6, 25°C) of $L^3Y(CH_2SiMe_3)_2THF$ (**5**).

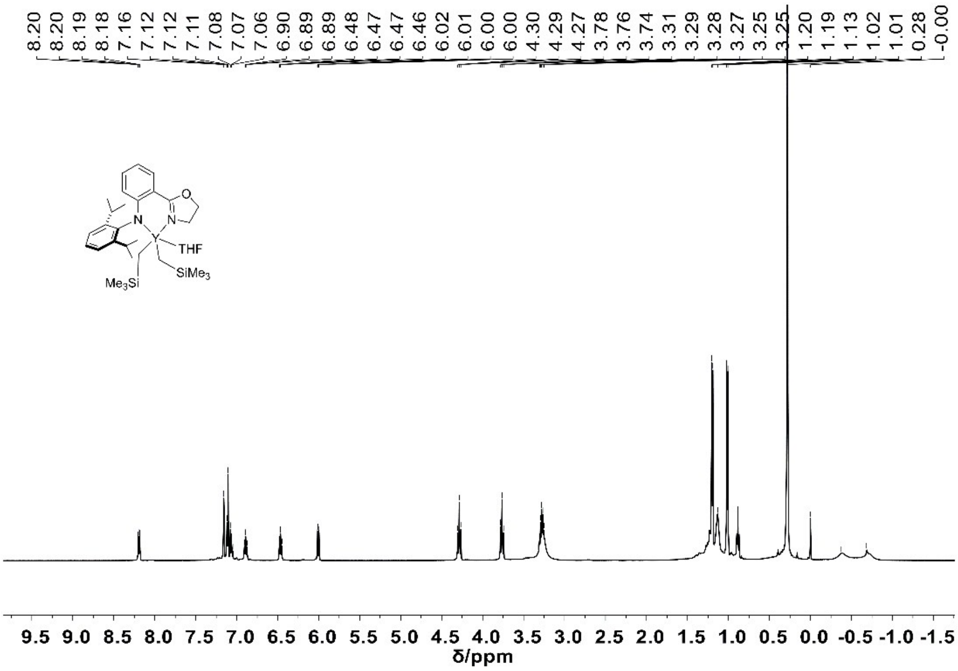

Fig. S15. ^{1}H NMR spectrum (500 MHz, C_6D_6, 25°C) of $L^4Y(CH_2SiMe_3)_2THF$ (**6**).

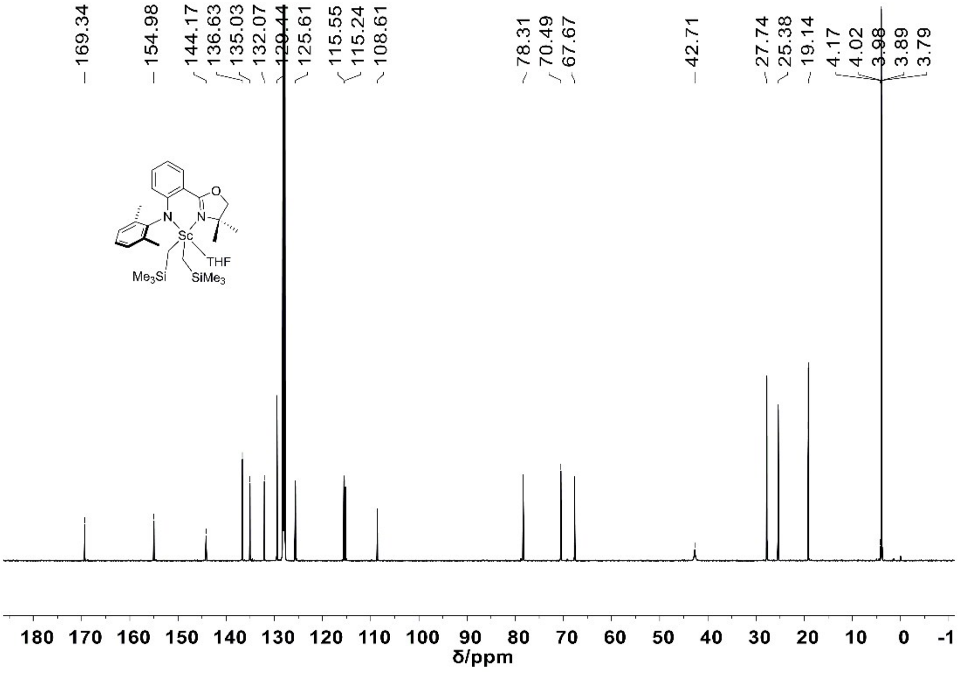

Fig. S16. ^{13}C NMR spectrum (125 MHz, C_6D_6, 25°C) of $L^1Sc(CH_2SiMe_3)_2THF$ (**1**).

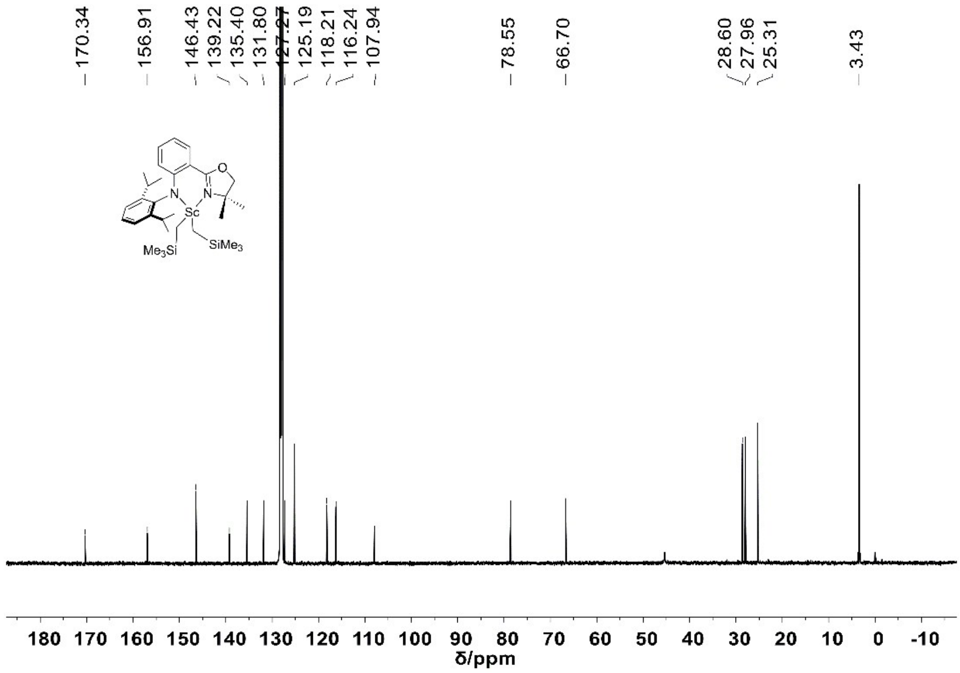

Fig. S17. ^{13}C NMR spectrum (125 MHz, C_6D_6, 25°C) of $L^2Sc(CH_2SiMe_3)_2$ (**2**).

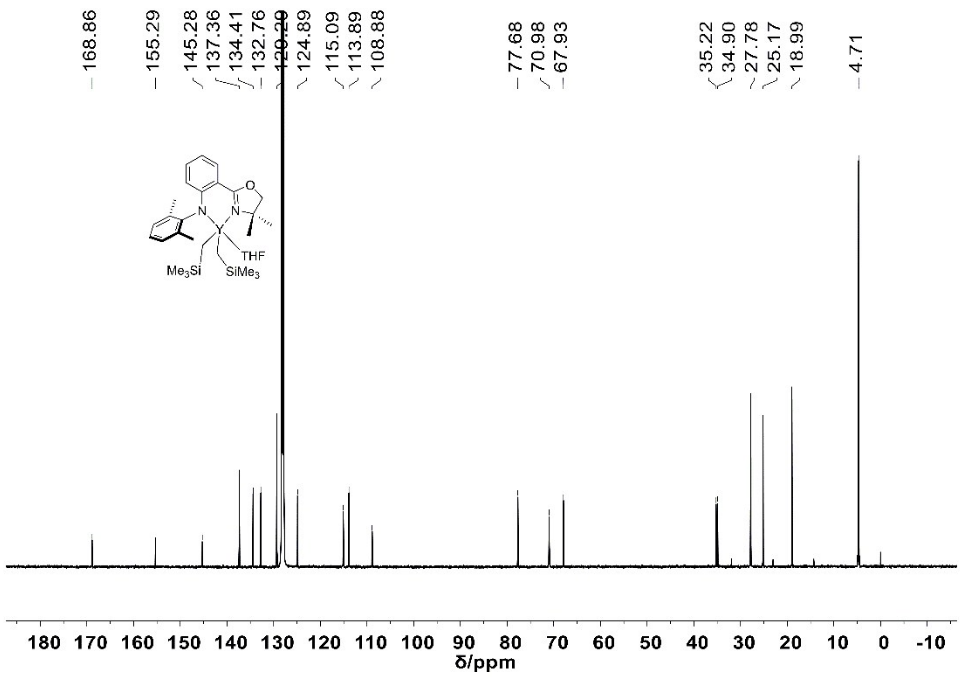

Fig. S18. ^{13}C NMR spectrum (125 MHz, C_6D_6, 25°C) of $L^1Y(CH_2SiMe_3)_2THF$ (**3**).

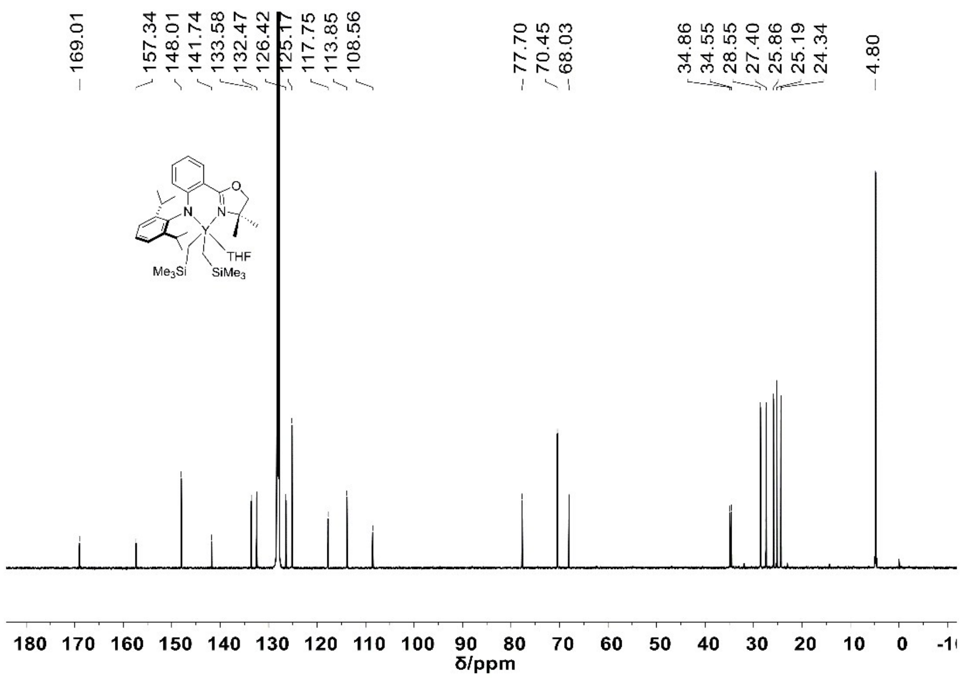

Fig. S19. ^{13}C NMR spectrum (125 MHz, C_6D_6, 25°C) of $L^2Y(CH_2SiMe_3)_2THF$ (**4**).

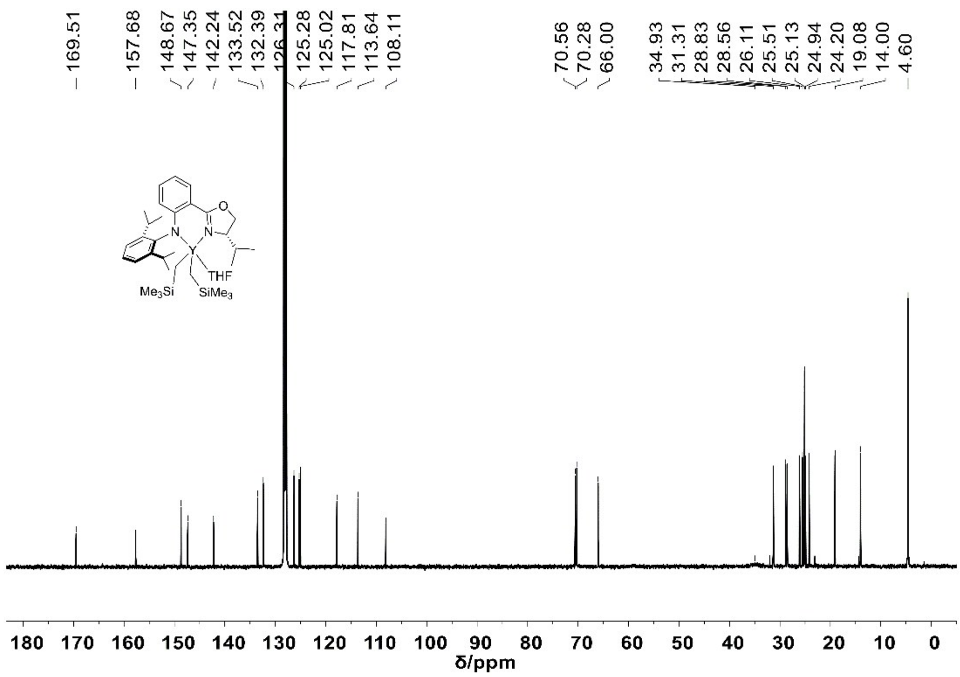

Fig. S20. ^{13}C NMR spectrum (125 MHz, C_6D_6, 25°C) of $L^3Y(CH_2SiMe_3)_2THF$ (**5**).

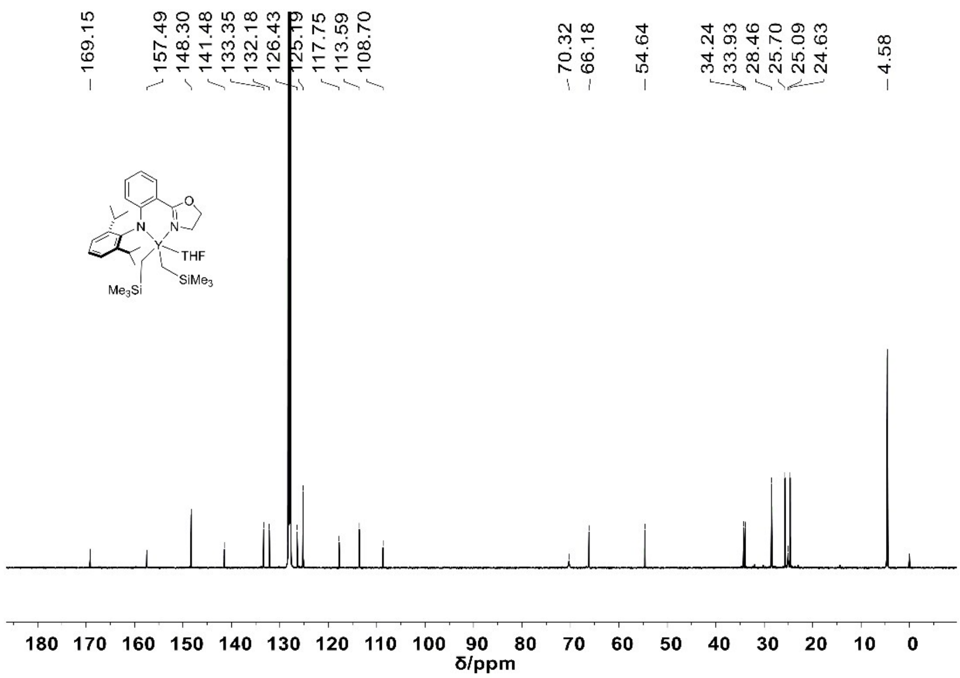

Fig. S21. ^{13}C NMR spectrum (125 MHz, C_6D_6, 25°C) of $L^4Y(CH_2SiMe_3)_2THF$ (**6**).

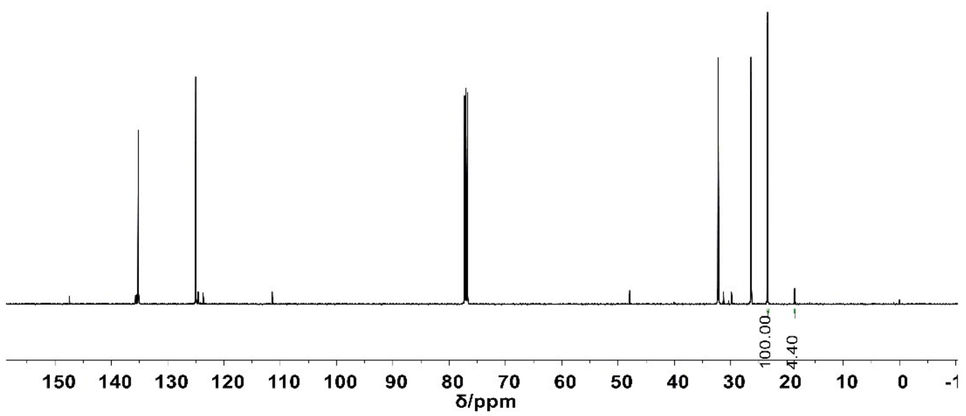

Fig. S22. ^{13}C NMR spectrum (125 MHz, $CDCl_3$, 25°C) of the resultant PIP (Table 4, run 1).

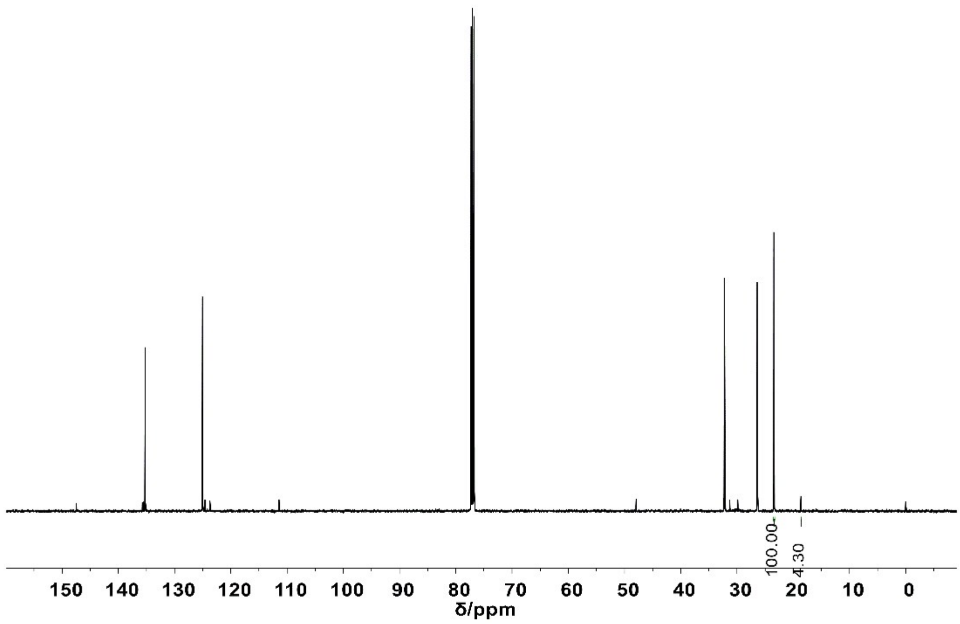

Fig. S23. ^{13}C NMR spectrum (125 MHz, $CDCl_3$, 25°C) of the resultant PIP (Table 4, run 2).

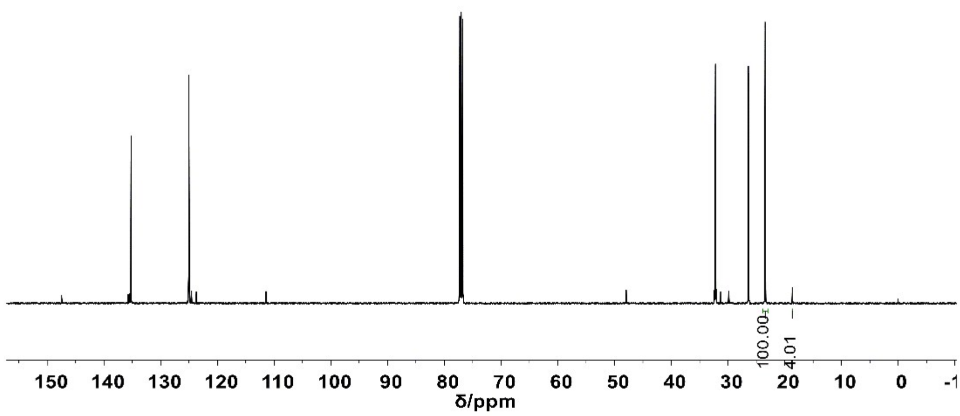

Fig. S24. ^{13}C NMR spectrum (125 MHz, $CDCl_3$, 25°C) of the resultant PIP (Table 4, run 3).

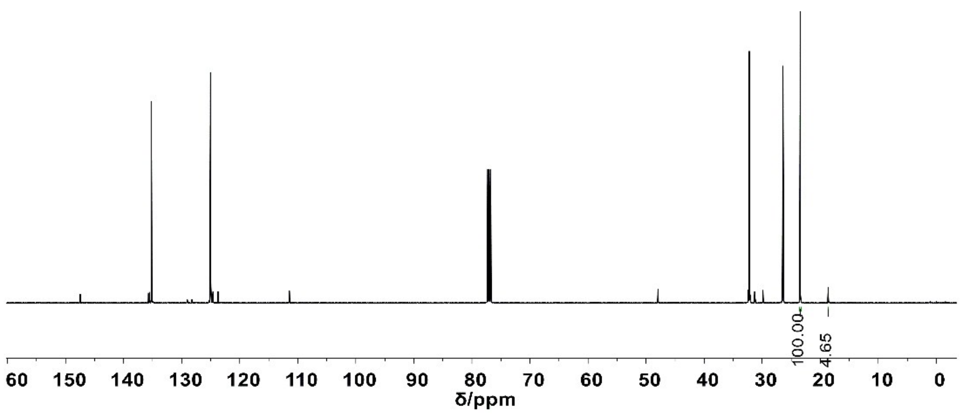

Fig. S25 ^{13}C NMR spectrum (125 MHz, $CDCl_3$, 25°C) of the resultant PIP (Table 4, run 4).

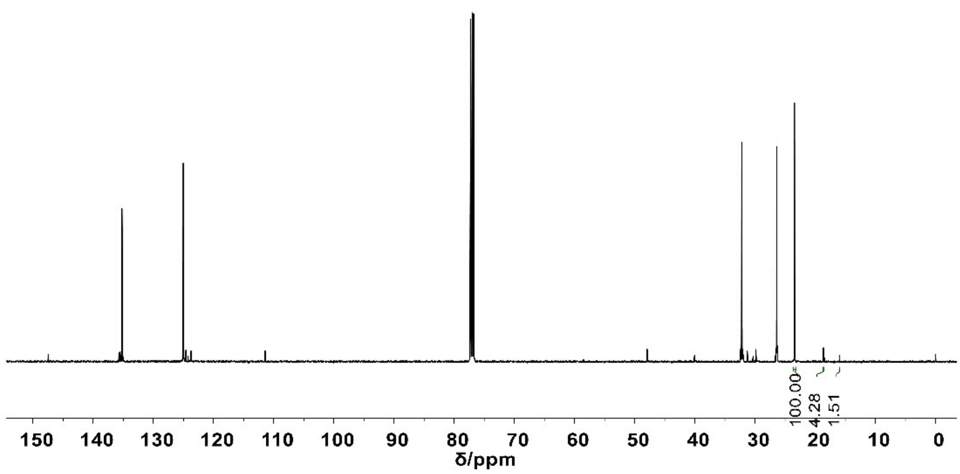

Fig. S26. ^{13}C NMR spectrum (125 MHz, $CDCl_3$, 25°C) of the resultant PIP (Table 4, run 9).

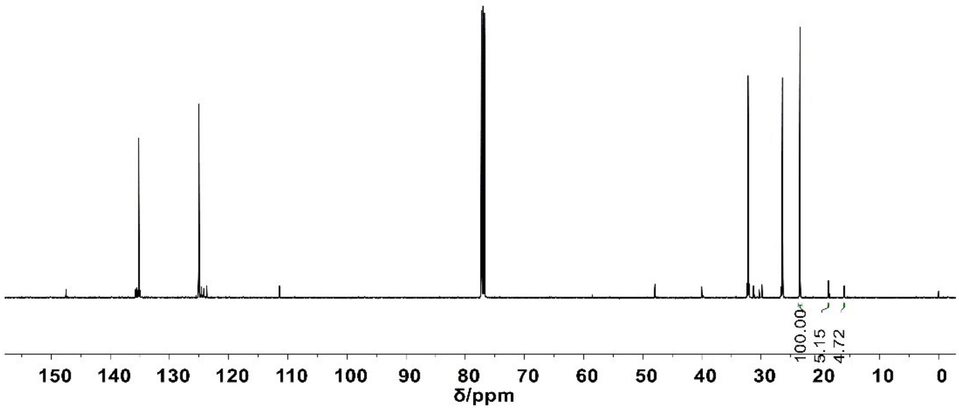

Fig. S27. ^{13}C NMR spectrum (125 MHz, $CDCl_3$, 25°C) of the resultant PIP (Table 4, run 10).

Table S1 Calculated electronic excitation energies (EEE) (eV) and corresponds oscillator strengths (OS) for complex **1** in the low-lying excited states.

States	EEE/eV	λ_{cal}/nm	OS	OT
S_1	3.454	359	0.1066	HOMO→LUMO
S_2	3.780	328	0.0162	HOMO-1→LUMO
S_3	4.105	302	0.0177	HOMO→LUMO+1
S_4	4.150	299	0.0087	HOMO-2→LUMO+1
S_5	4.250	292	0.0000	HOMO-1→LUMO+1

Table S2 Calculated electronic excitation energies (EEE) (eV) and corresponds oscillator strengths (OS) for complex **2** in the low-lying excited states.

States	EEE/eV	λ_{cal}/nm	OS	OT
S_1	3.271	379	0.1023	HOMO→LUMO
S_2	3.519	352	0.0163	HOMO-1→LUMO
S_3	3.861	321	0.0003	HOMO-2→LUMO+1
S_4	3.986	311	0.0039	HOMO→LUMO+1
				HOMO-1→LUMO+1

S_5	4.167	298	0.0013	HOMO-3→LUMO

Table S3 Calculated electronic excitation energies (EEE) (eV) and corresponds oscillator strengths (OS) for complex **3** in the low-lying excited states.

States	EEE/eV	λ_{cal}/nm	OS	OT
S_1	3.407	364	0.1167	HOMO→LUMO
S_2	3.770	329	0.0218	HOMO-1→LUMO
S_3	4.056	306	0.0143	HOMO→LUMO+1
S_4	4.086	303	0.0094	HOMO-2→LUMO
S_5	4.441	279	0.0060	HOMO→LUMO+3

Table S4 Calculated electronic excitation energies (EEE) (eV) and corresponds oscillator strengths (OS) for complex **4** in the low-lying excited states.

States	EEE/eV	λ_{cal}/nm	OS	OT
S_1	3.385	366	0.1080	HOMO→LUMO
S_2	3.736	332	0.0251	HOMO-1→LUMO
S_3	4.063	305	0.0151	HOMO-2→LUMO
				HOMO→LUMO+1
S_4	4.071	304	0.0163	HOMO-2→LUMO
				HOMO→LUMO+1
				HOMO→LUMO+2
S_5	4.326	287	0.0144	HOMO→LUMO+1
				HOMO→LUMO+2

Table S5 Crystallographic data and refinement details for complexes **7**.

	7·THF_2
Formula	$C_{64}H_{85}BN_2O_6SiY\cdot(C_4H_8O)_2$
formula weight	1250.41
Cryst. system	Monoclinic
Space group	*P*21/c
a (Å)	19.8165(19)
b (Å)	18.9374(19)
c (Å)	18.2758(18)
α(deg)	90
β(deg)	96.434(4)
γ(deg)	90
V (Å^3)	6815.2(12)
Z	4
R_{int}	0.0858
R_1	0.0839

wR_2	0.2636
Goof	1.0620